



## Reset-free adaptive polarization controller on a silicon-photonics platform for a self-coherent communication system

XUEFENG WANG,<sup>1,†</sup> YIFAN ZENG,<sup>1,†</sup> RUOLIN LIAO,<sup>1</sup> CAN ZHAO,<sup>1</sup> AND MING TANG<sup>1,2,\*</sup>

<sup>1</sup>Wuhan National Lab for Optoelectronics (WNLO) & National Engineering Laboratory for Next Generation Internet Access System, School of Optics and Electronic Information, Huazhong University of Science and Technology, Wuhan, 430074, China

<sup>2</sup>Optics Valley Laboratory, Hubei 430074, China

<sup>†</sup>These authors contributed equally to this work.

\*Corresponding author: tangming@mail.hust.edu.cn

Received 8 November 2022; revised 21 December 2022; accepted 6 January 2023; posted 9 January 2023; published 20 March 2023

To give full play to the advantages of the self-coherent systems in the data center scene, the problem of the random walk of the polarization state of the delivered local oscillator must be solved. An adaptive polarization controller (APC) is an effective solution, with the characteristics of easy integration, low complexity, being reset-free, and so on. In this work, we experimentally demonstrated an endlessly APC based on a Mach-Zehnder interferometer on a silicon-photonics integrated circuit. The APC is thermally tuned with only two control electrodes. It endlessly stabilizes the arbitrary state of polarization (SOP) of the light to a state of equal power of the two orthogonal polarizations (*X* and *Y*). A polarization tracking speed of up to 800 rad/s is achieved. © 2023 Optica Publishing Group

<https://doi.org/10.1364/OL.480516>

Self-coherent communication systems have attracted much attention recently for short-reach optical interconnects of inner or inter data centers (DCs) [1,2]. This allows the use of an uncooled laser with a large linewidth and significantly simplifies digital signal processing (DSP) algorithms by sending the modulated signal and a copy of the tone as a local oscillator (LO) originating from the same laser from the transmitter (Tx) [3]. However, the state of polarization (SOP) of the remotely delivered LO will fluctuate randomly, owing to the wake birefringence property of the single-mode fiber (SMF) and the influence of the unstable environment, and that may cause carrier fading in one of the polarizations (*X* or *Y*) after the polarization beam splitter, hence leading to failure in coherent reception. So, a specially designed adaptive polarization controller (APC) is needed to stabilize the varying SOP of the LO for the subsequent coherent detection. Compared with the situation in long-haul transmission links, in which fast polarization changes (up to several Mrad/s) may sporadically occur, such as caused by the lightning-induced strong magneto-optical effect, the polarization fluctuation in a DC network environment is expected to be much slower (below 100 rad/s [4]) because of the controlled environment in terms of both temperature and mechanical influences. Therefore, considering the cost and size in DC applications, the APC should have

a small insertion loss, a sufficient polarization tracking speed (not less than 100 rad/s), and a simple control system with low power consumption.

The APC can be implemented on various platforms, in the form of discrete components or integration. A discrete endless polarization controller may be based on either four rotatable quarter-wave plates (QWP), four wave plates with variable retardance, or fiber squeezers, oriented 45° from each other [5]. Lithium-niobate (LiNbO<sub>3</sub>) based solutions with a fast-tracking speed are also popular [6,7]. However, they are unsuitable for deployment in DC applications, considering the limited space and the sensitivity to cost.

For the ease of integration and cost reduction, a silicon (Si) photonic based solution is attractive. Generally, a Mach-Zehnder interferometer (MZI) based APC composed of two thermal phase shifters and two 3-dB couplers implemented on a Si-photonics integrated circuit (Si-PIC) is used to transfer any input SOP to the TE state [8,9]. Automated control algorithms are also designed to enhance the performance [10]. Moreover, the speed of thermal phase adjustment has been experimentally verified to be sufficient to deal with the polarization fluctuation in DC scenarios [4]. Meanwhile, the wide operation bandwidth of the Si-based APC enables it to be used in wavelength-division multiplexing (WDM) networks. However, reset operations are usually unavoidable once the driving signals reach the boundaries. To avoid the reset operation, more cascaded MZIs are needed [4,11]. As a result, the cost, power consumption, footprint, and algorithmic complexity increase significantly.

It is interesting to note that the carrier fading in the dual-polarization (DP) coherent communication system occurs only when the intensity of one of the orthogonal polarized LOs reaches zero; thus, the goal of the polarization stabilization could be simplified from TE SOP to the state of  $I_x = I_y$ , where  $I_x$  and  $I_y$  are the intensities of the orthogonally polarized light, which can be subsequently fed into the polarization-diversity coherent receiver. In this case, the structure and the control algorithm of the APC can be simplified. This idea was proposed in our previous work [3], where a scheme referred to as a LO polarization tracking integrated coherent receiver (PT-ICR) was

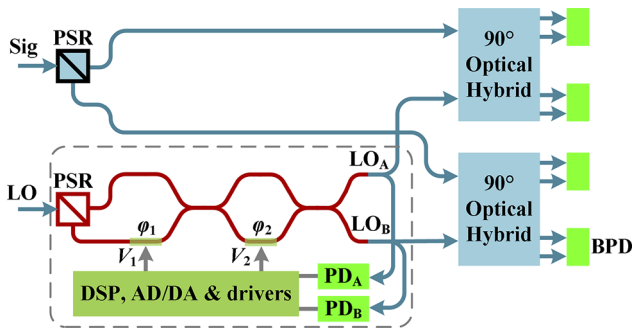


**Fig. 1.** Structure of LO PT-ICR.

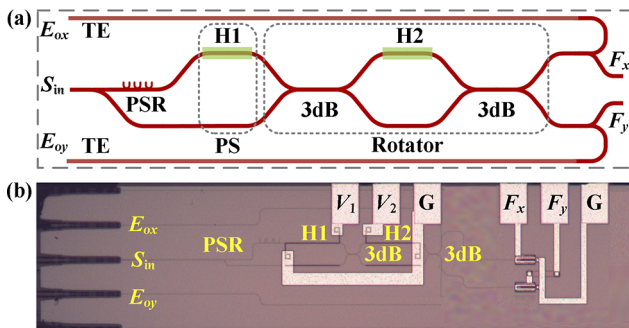


**Fig. 2.** (a) Layout of proposed APC. (b) Micrograph of fabricated chip. The size of the PIC is 1.2 mm × 0.4 mm. PS, phase shifter.

presented, as shown in Fig. 1. It is similar to the traditional coherent receiver with two polarization splitter-rotators (PSRs), two  $2 \times 4$  90° optical hybrids, and four balanced photodiodes (BPDs). A PIC (made with two stages of thermal phase shifters and two  $2 \times 2$  3-dB couplers) is placed after the LO port as the APC. However, reset operations still exist.

In this Letter, we propose an endless polarization stabilization algorithm applied on the same structure of the APC shown in Fig. 1 to stabilize the SOP to the state of  $I_x = I_y$ . The APC is separately implemented on the Si-PIC and can be easily integrated. Compared with our previous work [3], rigorous and detailed theoretical derivation and simulation verification were conducted. And with an upgraded driving circuit, the polarization tracking capacity is experimentally verified at a scrambling speed of up to 800 rad/s without reset operation.

Figure 2 shows the layout [Fig. 2(a)] and a micrograph [Fig. 2(b)] of the APC. The randomly polarized input light  $S_{in}$  is coupled into the Si-PIC using a low-loss edge coupler, followed by a polarization splitter-rotator (PSR), which separates and directs the TE and TM portions to the corresponding waveguide as a TE mode. Then, a MZI, composed of two thermal phase shifters,  $H_1, H_2$ , and two  $2 \times 2$  3-dB couplers, is designed to stabilize the amplitudes of the outputs of the PSR to be equal. The feedback signals  $F_x$  and  $F_y$  are about 10% of the intensity from the outputs  $E_{ox}$  and  $E_{oy}$ . The input and output ports are set at the same end and coupled with a fiber array (FA). The insertion losses of the two outputs from the input were measured as about 10.62 dB and 10.89 dB, respectively. By optimizing the coupling process, the insertion loss can be further reduced. It should be pointed out that this structure is easy to integrate with the ICR on the Si-PIC platform to form a PT-ICR with negligible additional insertion loss.

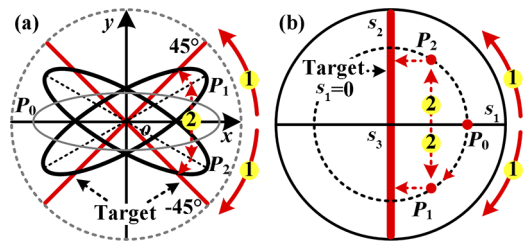


**Fig. 3.** SOP rotation and reset-free function of MZI-based APC: (a) in the Jones domain; (b) in the Stokes domain (top view).

The MZI is divided into two components. the first one, formed by  $H_1$ , acts as a phase shifter (PS), and the second one, composed of two 3-dB couplers sandwiching  $H_2$ , acts as a rotator. The SOP stabilization algorithm is similar to that proposed by Martinelli *et al.* [12]. The Jones expression of the procedure where the light passes through the MZI structure in the APC can be expressed as

$$\begin{bmatrix} E_{ox} \\ E_{oy} \end{bmatrix} = \frac{1}{2} \begin{bmatrix} 1 & j \\ j & 1 \end{bmatrix} \begin{bmatrix} e^{j\varphi_2} & 0 \\ 0 & 1 \end{bmatrix} \begin{bmatrix} 1 & j \\ j & 1 \end{bmatrix} \begin{bmatrix} e^{j\varphi_1} & 0 \\ 0 & 1 \end{bmatrix} \begin{bmatrix} E_{ix} \\ E_{iy} \end{bmatrix}, \quad (1)$$

where  $[E_{ix} \ E_{iy}]^T$  is the Jones vector of the input light, and  $\varphi_1$  and  $\varphi_2$  are the phase delay of the two thermal PSs. In the right-hand side of Eq. (1), the first part is the shared item, which can be ignored. The second part is a rotation matrix, describing the SOP rotation function of the rotator. The third part shows the phase delay introduced by  $H_1$ .

Then, the output can be calculated as

$$E_{ox} = e^{j\varphi_1} \sin\left(\frac{\varphi_2}{2}\right) E_{ix} + \cos\left(\frac{\varphi_2}{2}\right) E_{iy}, \quad (2)$$

$$E_{oy} = e^{j\varphi_1} \cos\left(\frac{\varphi_2}{2}\right) E_{ix} - \sin\left(\frac{\varphi_2}{2}\right) E_{iy} \quad (3)$$

The algorithm consists of two steps. In the first step, the arbitrary SOP  $P_0$  is rotated by the rotator to  $P_1$  near the target region  $I_x = I_y$ . Specifically, the angle between the long or short axis of the ellipse trajectory of the SOP  $P_1$  and the  $x$  axis should be near 45°, as shown in Fig. 3(a). From the view of the Stokes domain, as shown in Fig. 3(b), the arbitrary SOP  $P_0$  is rotated to  $P_1$  near the target region  $s_1 = 0$  (i.e.,  $I_x = I_y$ ) around the  $s_3$  axis. Most of the time, the target can be directly reached in the first step. At the second step (reset-free), once the phase value  $\varphi_2$  in the rotator reaches the boundaries ( $k\pi$  rad, where  $k$  is an integer), the outputs in Eqs. (2) and (3) become

$$E_{ox}|_{\varphi_2=2k\pi} = \pm E_{iy}, \quad E_{oy}|_{\varphi_2=2k\pi} = \pm e^{j\varphi_1} E_{ix}, \quad (4)$$

$$E_{ox}|_{\varphi_2=(2k-1)\pi} = \pm e^{j\varphi_1} E_{ix}, \quad E_{oy}|_{\varphi_2=(2k-1)\pi} = \mp E_{iy}. \quad (5)$$

It can be found that the intensities of the two outputs remain unchanged, even when  $\varphi_1$  is adjusted. At this moment, a  $\pm\pi$  rad phase change is imposed to  $\varphi_1$ , and the SOP  $P_1$  is switched to its symmetric state  $P_2$  with respect to the  $x$  axis (in the Jones domain) or rotated to  $P_2$  by  $\pi$  rad around the  $s_1$  axis (in the Stokes domain). Then the rotation direction of the rotator can be inversed while maintaining the locking status of  $s_1 = 0$ . Thus, the reset operation of  $\varphi_2$  is avoided.

The simulation results are shown in Fig. 4. The randomly scrambled SOP of the input light [Fig. 4(a)] is stabilized to the

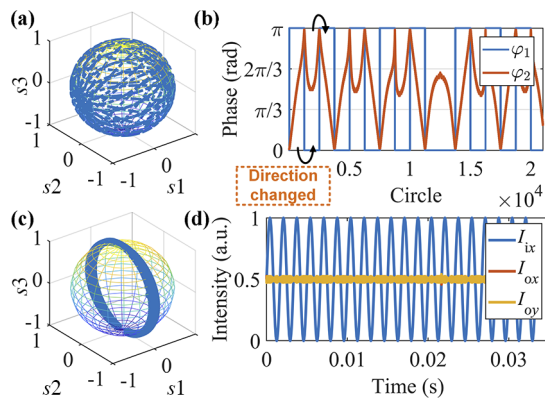


**Fig. 4.** Simulation results: (a) scrambled SOP; (b) control signals; (c) stabilized SOP; (d) intensities of orthogonal polarization components of input and output light.

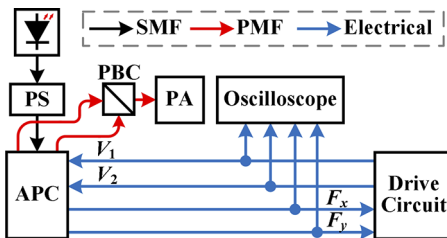


**Fig. 5.** Setup of testing system for MZI-based APC. PA, polarization analyzer; PBC, polarization beam coupler; PMF, polarization-maintaining fiber; PS, polarization scrambler.

target state [Figs. 4(c) and 4(d)] using the proposed algorithm. The reset-free operation is illustrated in Fig. 4(b). When  $\varphi_2$  reaches the boundary, 0 rad, its moving direction can be changed by adding or dropping  $\pi$  rad to  $\varphi_1$ . Thus, the reset operation of  $\varphi_2$  is avoided.

To verify the polarization tracking capability of the proposed APC, experiments were carried out. The setup is shown in Fig. 5. The continuous wave (CW) polarized light is generated by a laser (Koheras BASIK MIKRO E15, NKT) with less than 10 kHz linewidth and 13 dBm output power. Its SOP is scrambled using a polarization scrambler (EPS1000, Novoptel), then stabilized by the APC driven by an in-house developed circuit. The two output lights are coupled into a polarization beam combiner (PBC). Then, the SOP is analyzed by a polarization analyzer (PA) (General Photonics PolaDetect POD-101D). The signals  $V_1$  and  $V_2$  are the driving signals of the two heaters  $H_1$  and  $H_2$ , and  $F_x$  and  $F_y$  are the feedback signals. These four electrical signals are acquired using an oscilloscope (Picoscope 3000 series) and transmitted to a computer for further off-line analysis.

The phase delays of  $H_1$  and  $H_2$  are proportional to the applied powers according to the thermo-optic effect. To realize the proposed controlling algorithm, the adjustable phase range of  $H_1$  and  $H_2$  should cover at least  $[0, \pi]$  rad. As the key of the algorithm is to find the boundary of  $\varphi_2$  exactly, it is crucial to measure the half-wave power ( $P_\pi$ ) and the voltages corresponding to  $k\pi$  rad of  $H_1$  and  $H_2$ . The results are shown in Figs. 6(a) and 6(b).

First, we measured the boundary voltage of  $H_2$ , as shown in Fig. 6(b). As Eqs. (4) and (5) imply, when  $H_2$  reaches its boundary, the output optical power remains constant, no matter how  $\varphi_1$

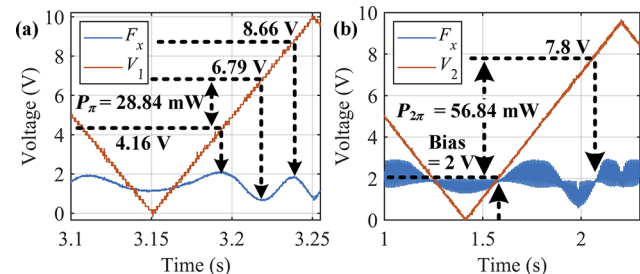


**Fig. 6.** (a) Measured results of half-wave power ( $P_\pi$ ) of  $H_1$ . (b) Results of  $H_2$ .

changes. In Fig. 6(b),  $V_2$  is increased from 0 V to 10 V in steps of 0.1 V, meanwhile,  $V_1$  is adjusted in the same way during the holding time of each value of  $V_2$ . The voltage 2 V corresponds to 0 rad, while 7.8 V corresponds to  $2\pi$  rad. Considering that the resistance of the two heaters is about  $1\text{ k}\Omega$ ,  $P_{2\pi}$  is calculated to be about 56.84 mW; thus,  $P_\pi$  is 28.42 mW. Second, the  $P_\pi$  of  $H_1$  is measured, as shown in Fig. 6(a), to determine the appropriate tuning range of  $V_1$ . To make the fluctuation of  $F_x$  more obvious with respect to  $\varphi_1$ ,  $\varphi_2$  is set at  $\pi/2$  rad by giving  $V_2$  a value of 5.69 V. Then, observing the fluctuation characteristics of  $F_x$  while increasing  $V_1$  from 0 V to 10 V,  $P_\pi$  of  $H_1$  is calculated to be about 28.84 mW by using the values of  $V_1$  corresponding to the two adjacent peak and valley values of  $F_x$ . The result of  $H_1$  is almost equal to that of  $H_2$ . We chose the voltages 4.16 V and 6.79 V as  $V_1$ .

Meanwhile, the response time (from 0 rad to  $\pi$  rad) of the two thermal PSs is measured to be about  $30\text{ }\mu\text{s}$ . Finally, the polarization stabilization capability is verified. The SOP of the light is scrambled by the three wave plates in the scrambler. These wave plates are two QWPs sandwiching one half-wave plate (HWP). The two QWPs rotate at a speed of 90 rad/s in opposite directions, and the HWP rotates at 800 rad/s. The HWP plays a major role in polarization rotation, while the two QWPs change the direction of polarization rotation, guaranteeing the worst case of polarization rotation.

The control algorithm aims to minimize the absolute value of the differential signal  $|s_1| = |(F_x - F_y)/(F_x + F_y)|$  to zero. The minimization process is achieved using a simple gradient descent algorithm with a fixed step on  $\varphi_2$ . There exist other algorithms that may improve the control robustness and speed [10], but that is beyond the scope of this Letter.

The experimental results are shown in Fig. 7(a). In the first half of the observation period, the APC is in off-mode, with a constant control voltage applied to  $H_1$  and  $H_2$ , and the feedback signals  $F_x$  and  $F_y$  fluctuate randomly. In the second half of the time, the APC is turned on, and  $F_x$  and  $F_y$  are stabilized to be equal. The control signal  $V_1$  switches between two voltages, corresponding to 0 rad and  $\pi$  rad, applied on  $\varphi_1$ , and  $V_2$  works in a limited range [2.0 V, 7.8 V] corresponding to the  $[0, 2\pi]$  rad phase range applied on  $\varphi_2$ . It can be seen that there is no reset operation applied to  $V_1$  or  $V_2$ . The common mode fluctuations of  $F_x$  and  $F_y$  are mainly caused by the polarization-dependent loss at the input port. The stabilizing process is dynamic rather than static and the feedback differential signal  $s_1$  continuously crosses the zero value under the algorithm. In Fig. 7(a),  $s_1$  is also calculated and can reflect the locking result. The maximum absolute value of  $s_1$  is 0.173. We define that the SOP is considered to be locked when  $|s_1|$  does not exceed 0.2. This means that the width of the ring of

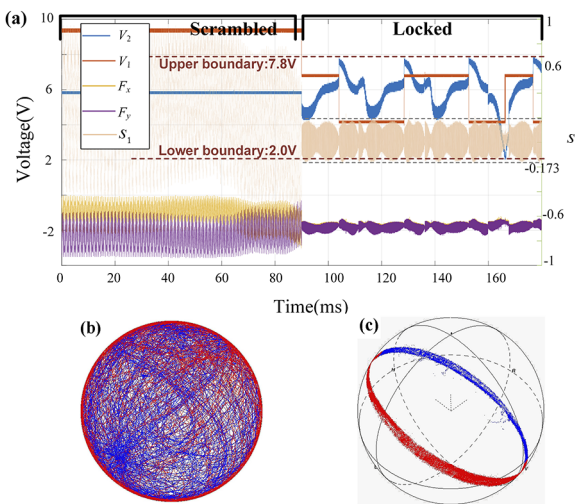


**Fig. 7.** (a) Polarization stabilization results with polarization rotation speed of about 800 rad/s. (b) Scrambled SOP. (c) Stabilized SOP.

$s_1 = 0$  shown in Fig. 7(c) does not exceed  $0.065\pi(\sin-1(0.2/1))$ . This locking state completely satisfies the needs of our further transmission experiments.

The phase jump operation of  $\varphi_1$  might introduce phase disturbance at the receiver. Fortunately, the response time of the thermal PS is about 30  $\mu$ s; thus, this kind of phase noise can be averaged among many symbols and will not affect the carrier phase recovery performance of the self-coherent system. It should be noted that this polarization stabilization algorithm has been successfully used in our published work [13], a real-time 600 G DP-64QAM demonstration of a homodyne coherent detection system with bidirectional transmission. A polarization rotation tracking speed of up to 800 rad/s is achieved without a performance penalty.

In conclusion, a silicon-photonic integrated APC capable of stabilizing any incoming SOP into the state of equal power of two polarizations ( $X$  and  $Y$ ) was designed and experimentally demonstrated. This APC model consists of two thermal PSs and two 3-dB couplers as one PS cascading a rotator. Stabilization of the different incoming SOPs is achieved by monitoring the optical power  $F_x$  and  $F_y$  with Ge-on-Si photodetectors and minimizing the differential signal by means of two thermal PSs,  $H_1$  and  $H_2$ . The minimization of  $s_1$  is realized by making  $s_1$  continuously cross zero. Most of the time, the rotator can enable the

stabilization target to be reached. Once the PS  $\varphi_2$  in the rotator touches the given boundaries ( $k\pi$  rad), a  $\pm\pi$  rad phase change is imposed on  $\varphi_1$ ; then the rotation direction of the rotator can be inverted, while the status of  $s_1 = 0$  is maintained. Thus, the reset operation is avoided. This reset-free APC, with a simple structure, two control electrodes, two feedback ports (which can be reduced to one by using a Ge-on-Si BPD), is recommended to eliminate carrier fading in a self-coherent communication system in the DC scenario. To deal with faster polarization fluctuations (even up to Mrad/s), meanwhile, taking size and cost into consideration, a thin-film LiNbO<sub>3</sub> [14] based endless APC will be a valuable subject for future research.

**Funding.** National Natural Science Foundation of China (61931010, 62225110).

**Disclosures.** The authors declare no conflicts of interest.

**Data availability.** Data underlying the results presented in this paper are not publicly available at this time but may be obtained from the authors upon reasonable request.

## REFERENCES

- M. Y. S. Sowailem, E. El-Fiky, M. Morsy-Osman, Q. Zhuge, T. M. Hoang, S. Paquet, C. Paquet, I. Woods, O. Liboiron-Ladouceur, and D. V. Plant, *Opt. Express* **25**, 27834 (2017).
- J. Cheng, C. Xie, Y. Chen, X. Chen, M. Tang, and S. Fu, in Optical Fiber Communication Conference (OFC) (2019), p. W1F.2.
- T. Gui, X. Wang, M. Tang, Y. Yu, Y. Lu, and L. Li, in Optical Fiber Communication Conference Postdeadline Papers (OFC-PDP) (2020), p. Th4C.3.
- A. Nespoli, G. Franco, F. Forghieri, M. Traverso, S. Anderson, M. Webster, and R. Gaudino, *IEEE Photonics Technol. Lett.* **31**, 62 (2019).
- N. G. Walker and G. R. Walker, *J. Lightwave Technol.* **8**, 438 (1990).
- B. Koch, A. Hidayat, H. Zhang, V. Mirvoda, M. Lichtinger, D. Sandel, and R. Noe, *IEEE Photonics Technol. Lett.* **20**, 961 (2008).
- R. Noé, B. Koch, and V. Mirvoda, in European Conference on Networks and Optical Communications (NOC) (2016), p. 162.
- M. Ma, K. Murray, M. Ye, S. Lin, Y. Wang, Z. Lu, H. Yun, R. Hu, N. A. F. Jaeger, and L. Chrostowski, in Conference on Lasers and Electro-Optics (2016), p. STu4G.8.
- J. N. Caspers, W. Yun, C. Lukas, and M. Mo, *Proc. SPIE* **9133**, 91330G (2014).
- .Minglei Ma, Hossam Shoman, Keyi Tang, Sudip Shekhar, Nicolas A. F. Jaeger, and Lukas Chrostowski, *Opt. Express* **28**, 1885 (2020).
- P. Oswald and C. K. Madsen, *J. Lightwave Technol.* **24**, 2932 (2006).
- M. Martinelli, P. Martelli, and S. M. Pietralunga, *J. Lightwave Technol.* **24**, 4172 (2006).
- T. Gui, X. Wang, M. Tang, Y. Yu, Y. Lu, and L. Li, *J. Lightwave Technol.* **39**, 1231 (2021).
- C. Wang, M. Zhang, X. Chen, M. Bertrand, A. Shams-Ansari, S. Chandrasekhar, P. Winzer, and M. Lončar, *Nature* **562**, 101 (2018).